ACS OMEGA

http://pubs.acs.org/journal/acsodf

Article

Polyaspartate Polyurea-Based Solid Polymer Electrolyte with High Ionic Conductivity for the All-Solid-State Lithium-Ion Battery

Lu Bai,[§] Peng Wang,*[,§] Chengyu Li, Na Li,* Xiaoqi Chen, Yantao Li, and Jijun Xiao*

Cite This: *ACS Omega* 2023, 8, 20272−20282

Read Online

ACCESS | Metrics & More | Article Recommendations | Supporting Information

ABSTRACT: The existing in situ preparation methods of solid polymer electrolytes (SPEs) often require the use of a solvent, which would lead to a complicated process and potential safety hazards. Therefore, it is urgent to develop a solvent-free in situ method to produce SPEs with good processability and excellent compatibility. Herein, a series of polyaspartate polyurea-based SPEs (PAEPU-based SPEs) with abundant $(PO)_x(EO)_y(PO)_z$ segments and cross-linked structures were developed by systematically regulating the molar ratios of isophorone diisocyanate (IPDI) and isophorone diisocyanate trimer (tri-IPDI) in the polymer backbone and LiTFSI concentrations via an in situ polymerization method, which gave rise to good interfacial compatibility. Furthermore, the in situ-prepared PAEPU-SPE@D_{15} based on the IPDI/tri-IPDI molar ratio of 2:1 and 15 wt % LiTFSI exhibits an improved ionic conductivity of 6.80×10^{-5} S/cm at 30 °C and could reach 10^{-4} orders of magnitude when the temperature was above 40 °C. The Lil$LiFePO_4$ battery based on PAEPU-SPE@D_{15} had a wide electrochemical stability window of 5.18 V, demonstrating a superior interface compatibility toward $LiFePO_4$ and the lithium metal anode, exhibited a high discharge capacity of 145.7 mAh g^{-1} at the 100th cycle and a capacity retention of 96.8%, and retained a coulombic efficiency of above 98.0%. These results showed that the PAEPU-SPE@D_{15} system displayed a stable cycle performance, excellent rate performance, and high safety compared with PEO systems, indicating that the PAEPU-based SPE system may play a crucial role in the future.

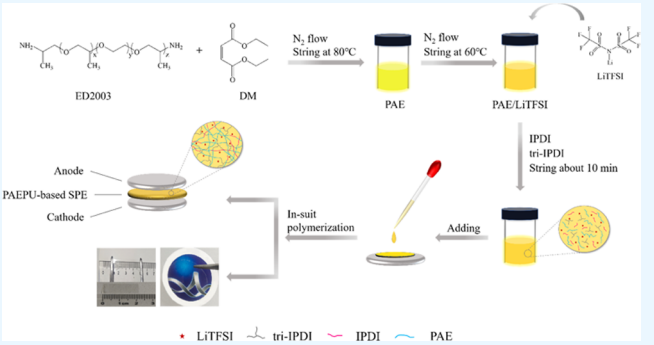

1. INTRODUCTION

Lithium-ion batteries (LIBs) have brought astonishing advancements and transformations in portable electronics and, more recently, electric vehicles during the past several decades.[1,2] With the rapidly expanding market of electric vehicles, storage systems with high energy density are in strong demand.[3−6] However, there are some serious safety issues such as short circuits, leakage, and combustion, even explosions, derived from the dendrite growth in liquid electrolytes.[7−9] Motivated by this challenge, many types of research such as solid-state inorganic electrolytes and solid polymer electrolytes (SPEs) have drawn significant attention.[10−15] The former mainly includes sulfide-based electrolytes and oxide-based electrolytes, which are brittle and have high interfacial resistance owing to poor contact with electrodes. In contrast, SPEs, blessed with a high flexibility and more safety, enable the application of a high-capacity Li−metal anode in which the possibility of internal short-circuiting by the penetration of dendritic Li can be suppressed. Consequently, SPEs may be the ultimate path to the batteries of the future.[16−18]

Most polymers have been recently exploited to dissolve lithium salts in these polymers for constructing SPEs, such as poly(ethylene oxide) (PEO), polyacrylonitrile (PAN), poly(vinylidene fluoride) (PVDF), poly(methyl methacrylate) (PMMA), and so on, in order to effectively enhance the performance of solid polymer electrolytes.[19−26] Especially, the SPE based on PEO is the most extensively investigated of polymer hosts for an efficient Li-salt dissolvability through the interaction of its ether oxygen bonds with cations. For all of the above reasons, numerous strategies have been reported to improve the ion conductivities of SPEs, including blocking[27−30] and grafting modification,[31,32] adding plasticizers,[33,34] polymer blending,[35,36] or forming the cross-networking.[37,38] Besides, many polymers containing abundant EO structure units have also been studied as matrices of SPEs.[39−43] In particular, the preparation methods of solid polymer electrolytes can influence the interface impedance. In addition to solution casting,[44,45] phase transformation,[46−48] and electrostatic spinning,[49,50] many researchers also often use in situ polymerization,[51−53] light curing methods,[54,55] and the scalable

Received: November 16, 2022
Accepted: April 11, 2023
Published: May 31, 2023

Scheme 1. Synthesis of PAEPU-Based SPE

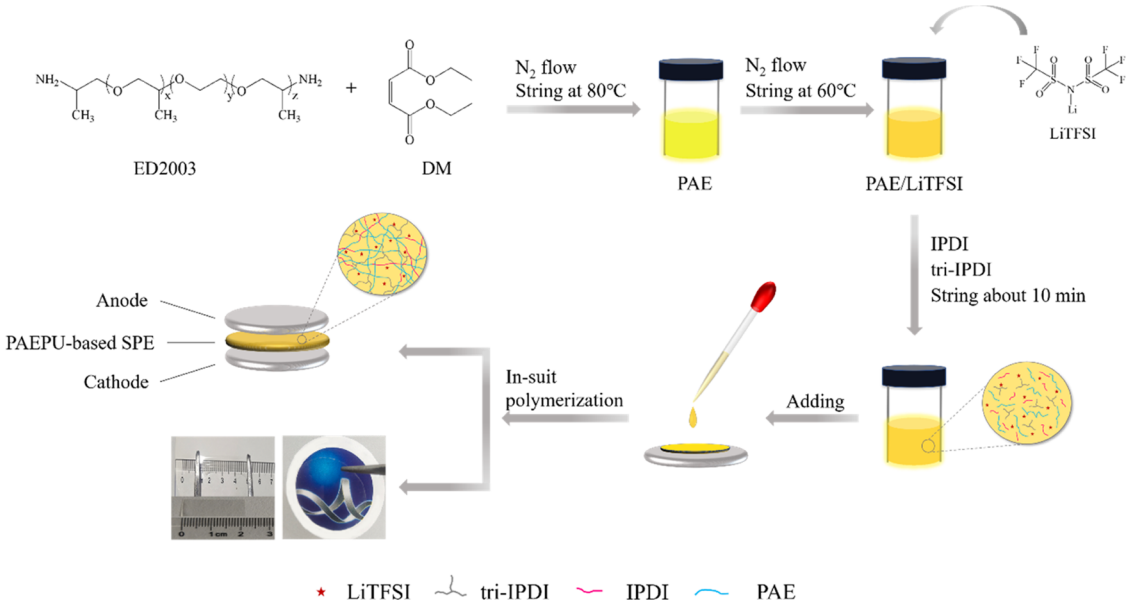

tape-casting method[56] to prepare solid polymer electrolytes. Zhao's research group[57] added the polymer matrix cellulose acetate (CA), the cross-linking agent poly(ethylene glycol diacrylate) (PEGDA), and the initiator AIBN to the liquid electrolyte, which consists of lithium hexafluorophosphate ($LiPF_6$), ethylene carbonate (EC), and diethyl carbonate (DEC); then, the layered boron nitride (BN) filler was added to the above mixture, and a cross-linked gel polymer electrolyte (GPE) was prepared by in situ thermal polymerization. The cross-linked GPE exhibits good mechanical and electrochemical properties, with an ionic conductivity of 8.9×10^{-3} S cm^{-1} at 30 °C and an electrochemical stability window of 5.5 V. Drews et al.[58] reported that the PIL brush-type GPE with PEtOx side chain was prepared by ultraviolet (UV) irradiation of a cationic vinylimidazolium-terminated poly(2-ethyl-2-oxazoline) (PEtOx) macromonomer and a multifunctional acrylic cross-linking agent dissolved in an organic electrolyte (LP30). In situ and ex situ preparation methods are used according to different characterizations, and the PIL brush GPE has good ionic conductivity, thermal properties, and electrochemical stability. Notwithstanding the organic solvents used in some systems of these gel electrolytes will be removed in subsequent operations,[59] the residual solvents may lead to side reactions with the electrodes. Apart from that, the residual organic solvents also increase the risk when working at higher temperatures, leading to safety issues that cannot be guaranteed. Consequently, it is necessary to develop a solvent-free solid electrolyte with EO structure.

Polyaspartate polyurea (PAEPU) is a kind of polymer rich in the ether oxygen group with good viscoelasticity and processing flexibility. The abundant ether oxygen groups endow it with a similar conduction mechanism to that of PEO. In addition, the raw materials are cheap and easy to obtain, and the preparation process of PAEPU is simple and does not need any organic solvent. These merits provide PAEPU the potential for use as a matrix of SPEs.

Herein, a solvent-free cross-linked PAEPU-based electrolyte with polyaspartic ester (PAE) and polyisocyanates as the main components was prepared by the in situ thermal polymerization method. Previously, the product of PAE and polyisocyanates was mostly used in the adhesive field,[60−62] but its use as an electrolyte has been scarcely reported. However, the PAEPU-based SPE membrane is expected to function as a novel electrolyte due to the following features: (i) the abundant ether oxygen bonds and low crystallinity are in favor of the transport of Li^+; (ii) formation of an integrated interface by in situ polymerization and strong adhesion to both electrodes; and (iii) the flexible and elastic properties can be tuned to accommodate the volume change originating from the anode. Besides, we are interested in a polymer matrix with a different cross-linking density; consequently, five different mole ratios of difunctional (isophorone diisocyanate (IPDI)) and trifunctional diisocyanate (isophorone diisocyanated trimer (tri-IPDI)), respectively, abbreviated as PAEPU-SPE@R_n, are employed in this study. Here, R refers to A, B, C, D, and E, which reflect the different mole ratios of IPDI to tri-IPDI (the ratios are 0:1, 1:2, 1:1, 2:1, and 3:1, respectively), and n refers to the mass concentrations (0, 5, 15, and 25 wt %) of LiTFSI, which are based on the mass of PAE. The thermal and electrochemical properties of the solvent-free solid-state polymer electrolyte were systematically studied. The results show that the PAEPU-based SPE has good stability and a wide electrochemical stability window, and there is low interface impedance between the electrode and electrolyte due to the in situ polymerization method. Beyond the obvious benefits already discussed, the electrolytes show outstanding comprehensive properties, and the cells assembled with the electrolytes exhibit superior electrochemical performances.

2. EXPERIMENTAL SECTION

2.1. Materials. Polyetheramine (ED2003 $M_w \approx 2000$) was purchased from Shandong Mole Chemical Co., Ltd. Diethyl maleate (DM) was purchased from Guangzhou Yuanda New Material Co., Ltd. Isophorone diisocyanate (IPDI) was purchased from Wuhan Kanos Technology Co., Ltd. Isophorone diisocyanated homopolymer (IPDI-trimer) was purchased from Jining Huakai Resin Co., Ltd. Lithium bis(trifluoromethanesulfonyl)imide (LiTFSI) was purchased from Aladdin (Shanghai, China) and used as received. *N*-methylpyrrolidone (NMP), lithium iron phosphate ($LiFePO_4$),

https://doi.org/10.1021/acsomega.2c07349
ACS Omega 2023, 8, 20272−20282

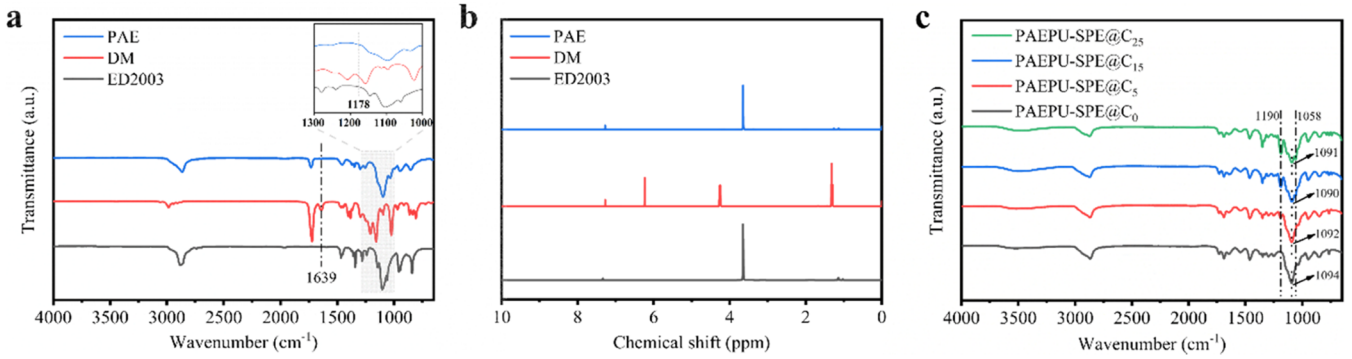

Figure 1. (a) FT-IR and (b) ^{1}H NMR spectra of PAE, DM, and ED2003. (c) FT-IR spectra of PAEPU-SPE@C$_n$ (n = 0, 5, 15, 25).

poly(vinylidene fluoride) (PVDF), and carbon black (Super P) were procured from Guangdong Canrd New Energy Technology Co., Ltd.

2.2. Preparation of PAE. The PAE was synthesized through the Michael reaction using ED2003 and DM. Into a four-necked flask was added ED2003 (50 g, 0.025 mol) with stirring and using a thermometer; then, DM was added dropwise (8.61 g, 0.05 mol) under N_2 atmosphere; the temperature of the mixture was kept below 60 °C during the dripping process. Subsequently, the mixture was heated to 80 °C and stirred at this temperature for 24 h.

2.3. Preparation of PAEPU-Based SPEs. PAE was mixed with different contents of LiTFSI at 60 °C for 12 h to obtain the mixed solution of PAE/LiTFSI in a dried N_2 atmosphere. The PAE/LiTFSI mixture was reacted with a stoichiometric amount of polyisocyanates in a Teflon beaker by magnetic stirring for about 10 min. Subsequently, the final solution was cast onto a PP board using a scraper. After reacting in a dry environment at 60 °C for at least 12 h, a series of soft and viscoelastic PAEPU-based SPEs was prepared. The thickness of PAEPU-based SPEs was about 150 μm.

Different preparation processes were selected according to the characterization methods: (1) In order to carry out Fourier-transform infrared (FT-IR), scanning electron microscopy (SEM), energy dispersive X-ray spectroscopy (EDS), X-ray diffraction spectroscopy (XRD), differential scanning calorimetry (DSC), and thermogravimetric analysis (TGA) characterization, an evenly mixed electrolyte was coated on a dry flat polypropylene plate with a scraper, placed at room temperature for 5 h, and then transferred to a vacuum oven at 60 °C for 24 h; after curing, the electrolyte was transferred to a nonstick paper for storage. (2) For the rheological property test, the evenly mixed electrolyte was directly coated on the parallel-plate clamp for testing. (3) In order to test the ionic conductivity, electrochemical stability window, ion migration number, interface stability, cycle life, rate performance, and application, the uniformly mixed electrolyte was directly polymerized in situ on stainless steel, lithium, or cathode plates. The synthesis of PAEPU-based SPE is shown in Scheme 1.

2.4. Assembly of the Symmetrical, Unsymmetrical, and Half Cells. For electrochemical testing, the batteries are divided into several types to assemble. Symmetric batteries are used in the AC impedance test; a solid polymer electrolyte (SPE) caught in the middle of a stainless steel shrapnel (SS) or metallic lithium pills (Li) forms the "sandwich" structure: SS/SPE/SS or Li/SPE/Li, respectively. Asymmetric batteries assembled with Li/SPE/SS are used in the linear sweep voltammetry test. The half-cell assembled with Li/SPE/$LiFePO_4$ is utilized for testing the other batteries' performance. All types of cells were assembled with the CR2032 coin type in a glovebox (H_2O < 0.1 ppm, O_2 < 1 ppm) under Ar atmosphere. In addition, the preparation of the $LiFePO_4$ cathode is described in Supporting Information.

2.5. Characterization. The structures of the PAE and the PAEPU-based SPE were tested by Fourier-transform infrared spectroscopy (FT-IR IRL280301, Perkin Elmer) from 650 to 4000 cm^{-1} and ^{1}H NMR spectroscopy (Avance III HD 400MHz, Bruker, Germany), which used deuterated chloroform ($CDCl_3$) as the standard solvent. The dynamic process of the PAEPU-based SPE at 60 °C with an angular frequency of 10 rad/s was determined through the small-amplitude time scanning mode in the rotary rheometer (DHR-1, TA) oscillation test. The mechanical behavior of the PAEPU-based SPE was characterized using a small-amplitude frequency scanning mode in a rotary rheometer oscillation test with a 25 mm aluminum parallel-plate geometry at 80 °C, and the frequency sweeps were performed at a controlled strain of 1.0% from 500 to 0.1 rad/s. The surface morphologies of the SPE were investigated using a scanning electron microscope (SEM) (Inspect-S50, FEI). The surface element distribution of the SPE was characterized by energy dispersive X-ray spectroscopy (EDS) (EDAX APOLLP XL, AMETEK) and the crystallinity change of the SPE was analyzed by X-ray diffraction spectroscopy (XRD) (D/MAX-2500, Rigaku, Japan) in the diffraction angle range from 2 to 100°. The thermal transition of the SPE was measured by differential scanning calorimetry (DSC) (Germany Netzsch DSC 214) with a scan rate of 20 °C/min under N_2 atmosphere from −100 to 100 °C. The thermal properties of the SPE were measured by thermogravimetric analysis (TGA) (Q50, TA) under N_2 atmosphere at a heating rate of 20 °C/min.

Ionic conductivity is one of the most important properties of lithium batteries, which is calculated by $\sigma = \frac{d}{R_b S}$, where d is the thickness of the PAEPU-based SPE, R_b is the bulk resistance, and S is the effective area. R_b was obtained by electrochemical impedance spectroscopy (EIS) in the frequency range of 10^6–1 Hz with an amplitude of 10 mV.

The electrochemical stability window was measured by linear sweep voltammetry (LSV), with the voltage ranging from 2 to 6 V at a scanning rate of 10 mV/s. The lithium-ion transference number (t_{Li^+}) of the PAEPU-based SPE was evaluated by the formula $t_{Li+} = \frac{I^s R_b^s (\Delta V - I^0 R_i^0)}{I^0 R_b^0 (\Delta V - I^s R_i^s)}$. The cell was polarized by a DC voltage (ΔV) at 10 mV, and the initial (I_0)

https://doi.org/10.1021/acsomega.2c07349
ACS Omega 2023, 8, 20272−20282

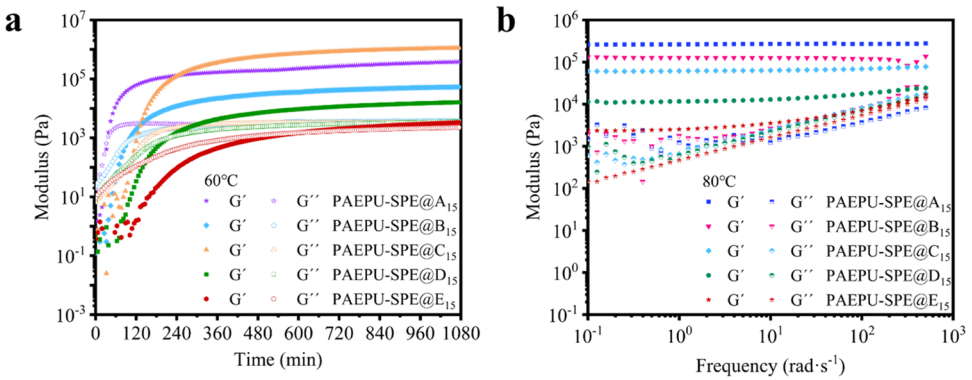

Figure 2. (a) Modulus−time curve of PAEPU-SPE@R_{15}. (b) Modulus−frequency curve of PAEPU-SPE@R_{15}.

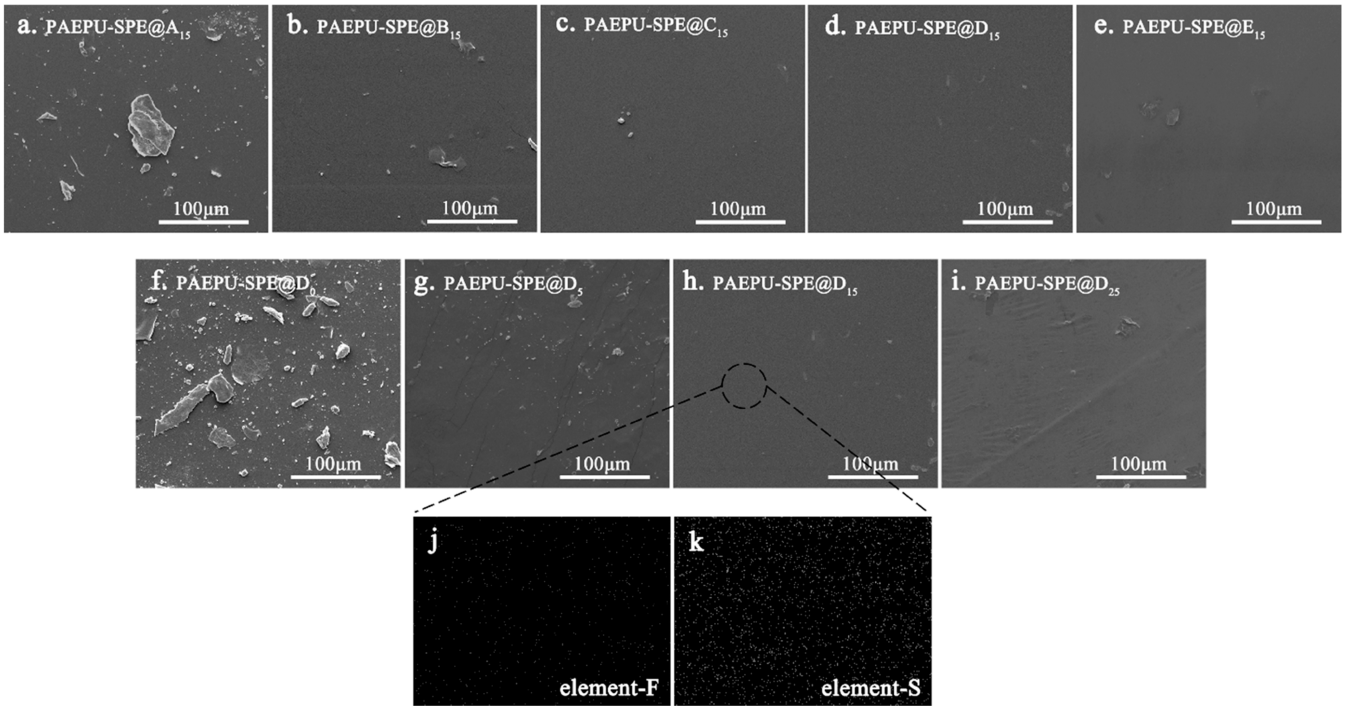

Figure 3. SEM images and EDS mapping images of PAEPU-based SPE. (a−e) SEM images of PAEPU-SPE@R_{15}. (f−i) SEM images of PAEPU-SPE@D_n (n = 0, 15). (j−k) EDS mapping images of PAEPU-SPE@D_{15}.

and steady-state (I_s) currents were measured. In this formula, R_b^0 and R_b^s are the bulk resistances before and after the polarization; R_i^0 and R_i^s are the corresponding interface resistances before and after the polarization. All of the resistances were acquired by EIS over a frequency ranging from 10^6 to 10^{-1} Hz with an amplitude of 10 mV.

To evaluate the interfacial stability and compatibility of the PAEPU-based SPE and lithium metal, an Li/PAEPU-based SPE/Li lithium symmetric battery system was assembled to monitor the change of interface impedance over time. The interface resistances were acquired by EIS with a 10 mV amplitude over the frequency ranging from 10^6 to 1 Hz.

The cycling performance of the Li/PAEPU-based SPE/LFP half-cell was determined with a voltage range of 2.5−3.8 V and a current density of 0.5C at 60 °C using a battery tester (CT2001A, LANHE System, China). The rate capabilities of the Li/PAEPU-based SPE/LFP half-cell were determined in the voltage range of 2.5−3.8 V at current densities of 0.1C, 0.2C, 0.5C, 1C, and 2C, respectively, at 60 °C using a LAND battery tester.

3. RESULTS AND DISCUSSION

3.1. FT-IR and ^{1}H NMR Characterization. The structure of PAE was identified by FT-IR and ^{1}H NMR spectra. In the FT-IR spectra (Figure 1a), an absorption peak corresponding to C−O−C was observed at 1094 cm^{-1}, while the absorption at 1639 cm^{-1} attributed to the C═C in the DM disappeared, verifying the formation of PAE. Moreover, the ^{1}H NMR spectrum of PAE showed a peak at 3.68 ppm (Figure 1b) assigned to the proton of −CH_2O−, and the peak at 6.28 ppm assigned to the protons of −CH═CH− in DM disappeared.

Figure 1c shows the FT-IR spectra of PAEPU-SPE@C_n (n = 0, 5, 15, 25). New absorption peaks of S═O and C−F were observed at 1058 and 1190 cm^{-1}, respectively; the absorption corresponding to the C−O−C in the main chain was observed at about 1094 cm^{-1}, in which the abundant ether oxygen groups (−C−O−C−) were conducive to lithium-ion transmission. The absorption of C−O−C in PAE with lithium salt drifted toward 1090 to 1092 cm^{-1}. The resulting data are due to the interaction between Li^+ and C−O−C, that is, the

https://doi.org/10.1021/acsomega.2c07349
ACS Omega 2023, 8, 20272−20282

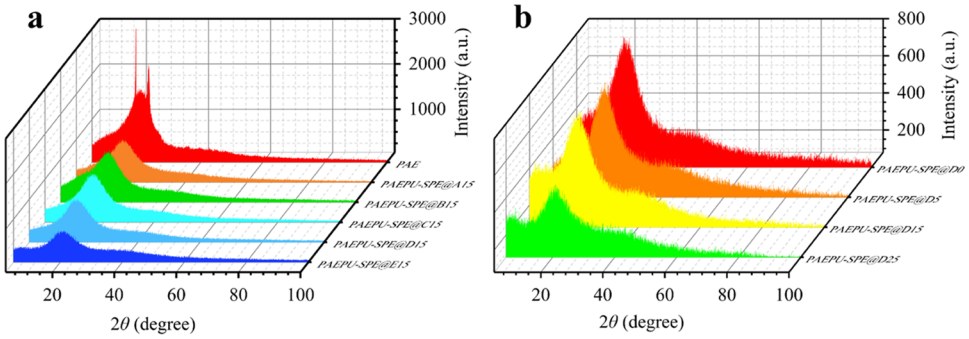

Figure 4. (a) XRD pattern of PAEPU-SPE@R_{15} (R = A, B, C, D, E). (b) XRD pattern of PAEPU-SPE@D_n (n = 0, 5, 15, 25).

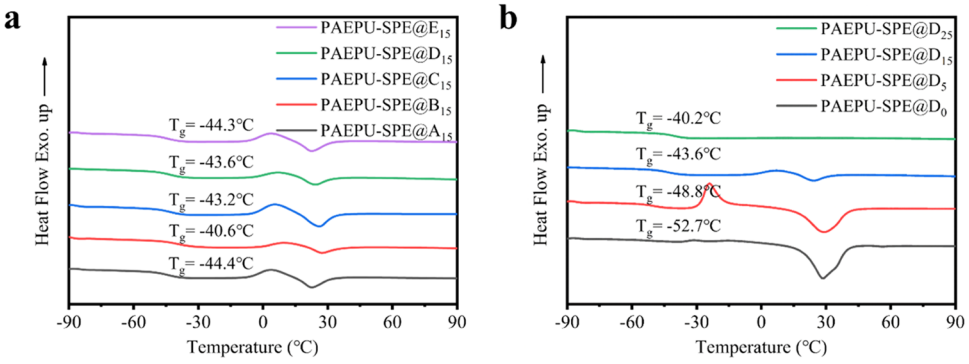

Figure 5. DSC analysis of (a) PAEPU-SPE@R_{15} (R = A, B, C, D, E) and (b) PAEPU-SPE@D_n (n = 0, 5, 15, 25).

formation of ion-dipole complexation, resulting in the C−O−C stretching band shifting to a low wavenumber. This phenomenon is also often observed in the PEO system.[63]

3.2. Viscoelastic Behavior. Take PAEPU-SPE@R_{15} as an example. Figure 2 shows the viscoelastic behavior of PAEPU-based SPEs. The storage modulus (G') and the loss modulus (G''), which denote the elastic and viscous properties of PAEPU-SPE@R_{15}, respectively, were tested using a rheometer at a certain temperature. Figure 2a shows the dynamic changes of the modulus for PAEPU-SPE@R_{15} with the reaction time at 60 °C and 10 rad/s. As the reaction time increases, G' and G″ increase, indicating that PAEPU-SPE@R_{15} forms gradually. At the beginning of the reaction, G″ is obviously larger than G', demonstrating that the viscous property dominates the behavior of PAEPU-SPE@R_{15}, and PAEPU-SPE@R_{15} behaves more like a viscous liquid. G' even exceeds G″ up to one or two orders of magnitude after reaching the intersection of $G'-t$ and G″$-t$ curves, at which point PAEPU-SPE@R_{15} exhibits more elastic behaviors. As time continues, G' and G″ gradually tend to be stable, indicating that the reaction is basically over. The time taken to reach the intersection of $G'-t$ and G″$-t$ curves becomes short with the increase of tri-IPDI content, indicating that the cross-links inside PAEPU-SPE@R_{15} are crucial for determining its behavior.

The SPE with viscoelastic properties is favorable for the even deposition of metallic lithium, and prevent the formation of lithium dendrite. Therefore, the oscillatory shear rheology of PAEPU-SPE@R_{15} was studied to understand the viscoelastic properties. Results from oscillatory shear measurements at a fixed strain (γ = 1.0%) and variable dynamic frequency (ω) are shown in Figure 2b. All of the above measurements were taken at 80 °C. Interestingly, for all PAEPU-SPE@R_{15} samples, the G' values are larger than the G″ values in the low-strain, linear viscoelastic regime, and the G' is independent of the frequency, demonstrating that the materials possess solid-like elastic consistency. In addition, it is found that the G' increases and the dependence of G″ on frequency decreases with the increase of cross-linking density. Viscoelasticity is beneficial to the uniform deposition of lithium dendrite and conducive to the performance of the battery.

3.3. Morphology and Physicochemical Properties. As shown in Figure 3, the surface morphology of the polymer electrolyte was probed by SEM. Figure 3a−e shows the SEM images of PAEPU-SPE@R_n (R = A, B, C, D, E; n = 15). It can be noted that the microgel content of the surface of PAEPU-SPE@R_n decreases with decrease of the tri-IPDI content at the same content of lithium salt and with the increase of the content of lithium salt at a fixed ratio of IPDI to tri-IPDI, and there are few gel substances in PAEPU-SPE@D_{15} and PAEPU-SPE@D_{25}. This may be because the lithium salt plays a certain "spacing role" in the polymerization process, which slows down the reaction speed between −NH and −NCO. When the content of lithium salt is too high, the contact probability of the two groups is reduced, resulting in inadequate reaction and surface wrinkling defects. Figure 3j,k, respectively, shows the EDS characterization of the unique elements (S and F element) in the lithium salt. The S and F elements are evenly distributed, verifying the uniform dispersion of the lithium salt in the SPE.

The transportation of lithium ions mainly relies on the movement of the chain segments, which mainly occurs in the amorphous area. The lithium-ion transmission can be more intuitively understood through the XRD pattern. In order to find out the reason for the improved Li^+ conduction, XRD was carried out on the PAE membrane, PAEPU-SPE@R_{15} (R = A, B, C, D, E), with different molar ratios of IPDI to tri-IPDI and PAEPU-SPE@D_n (n = 0, 5, 15, 25) and different concentrations of LiTFSI (Figure 4). It can be seen from

https://doi.org/10.1021/acsomega.2c07349
ACS Omega 2023, 8, 20272−20282

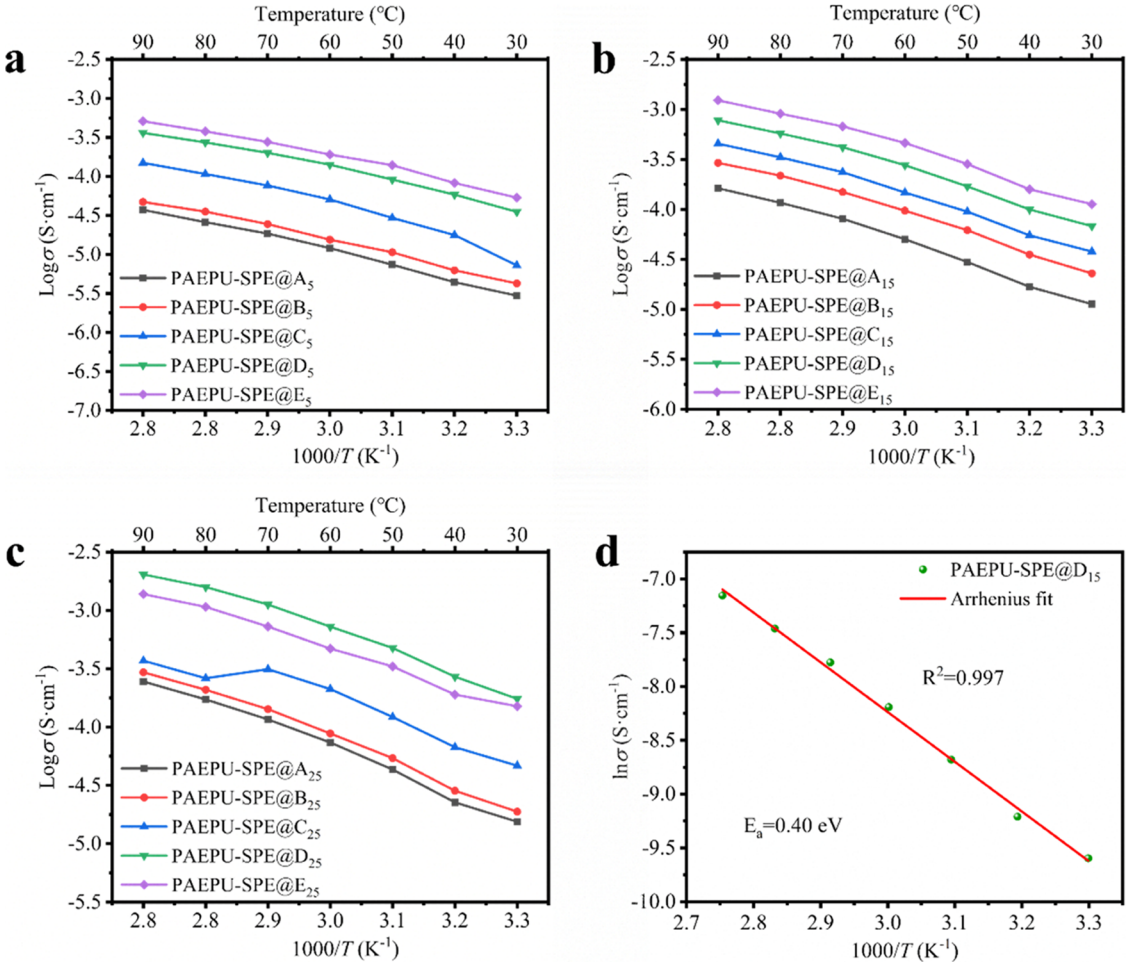

Figure 6. (a–c) Temperature dependence of the ionic conductivity of the PAEPU-based SPE, PAEPU-SPE@R_5 (R = A, B, C, D, E), PAEPU-SPE@R_{15} (R = A, B, C, D, E), and PAEPU-SPE@R_{25} (R = A, B, C, D, E). (d) Linear fitting of ln σ using the Arrhenius model with T = 303.15K.

Figure 4 that the diffraction peaks for the crystalline PEO chain segments in PAE are located at 19.1 and 23.3°; nevertheless, the diffraction peaks of PAEPU-SPE@R_{15} and PAEPU-SPE@D_n are widened and become diffusion peaks due to the cross-linking structure in PAEPU-based SPE, which restricts the formation of crystallization, creating more amorphous regions with the increase in molar ratio of tri-IPDI to IPDI or LiTFSI content. Furthermore, there are no diffraction peaks at 2θ of 19.1 and 23.3° for PAEPU-SPE@R_{15} and PAEPU-SPE@D_n, respectively; this may be because the intense diffraction peaks of PAEPU-based SPE mask the diffraction peaks at 19.1 and 23.3°. The DSC experimental data confirmed that there are melting points in PAEPU-based SPE except PAEPU-SPE@D_{25}.

The thermal transitions of the PAEPU-based SPE were investigated by differential scanning calorimetry (DSC). Figure 5a displays the heat flow as a function of temperature for PAEPU-based SPEs with different molar ratios of the IPDI to tri-IPDI ranging from 0:1 to 3:1 at 15 wt % of LiTFSI. It can be seen that the melting temperatures (T_m) and glass transition temperature (T_g) gradually reduced from PAEPU-SPE@B_{15} to PAEPU-SPE@E_{15} with the increase in the molar ratios of IPDI to tri-IPDI, indicating that the cross-linking disrupted the crystallization tendency of PAEPU-based SPEs. Nevertheless, PAEPU-SPE@A_{15} displayed the lowest T_g of −44.4 °C and T_m of 25 °C. It may be that there was tri-IPDI only, resulting in the viscosity increasing rapidly at the beginning of the reaction, which hinders the movement of chain segments and monomers to restrain the consequent reaction between PAE and tri-IPDI to affect the mechanical strength of PAEPU-based SPEs. Moreover, Figure 5b shows that the dosage of LiTFSI affects the T_m and T_g. The decrease in T_m and the increase in T_g indicate a transition from less to more interactions between the ions in LiTFSI and PEO chain segments. Especially, at 25 wt % of LiTFSI, the crystallization peak disappeared completely. This observation heralds a completely disrupt crystallization of PEO chain segments. As a result, the chain segment is more active, facilitating lithium-ion transfer and achieving higher ionic conductivity. In addition, the PAEPU-based SPEs exhibited outstanding thermal stability and the thermal decomposition temperature of 5% weight loss was above 300 °C, showing excellent stability under the condition of thermal abuse displayed in Figure S1a,b.

3.4. Electrochemical Performance Characterization.

Ionic conductivity has been identified as the most important means of characterizing the electrochemical properties of polymer electrolytes. In this paper, the influences of different LiTFSI content and different molar ratio of IPDI to tri-IPDI on the ionic conductivity of the PAEPU-based SPE were discussed. Figure 6 shows the curve of ionic conductivity changing with temperature.

https://doi.org/10.1021/acsomega.2c07349
ACS Omega 2023, 8, 20272−20282

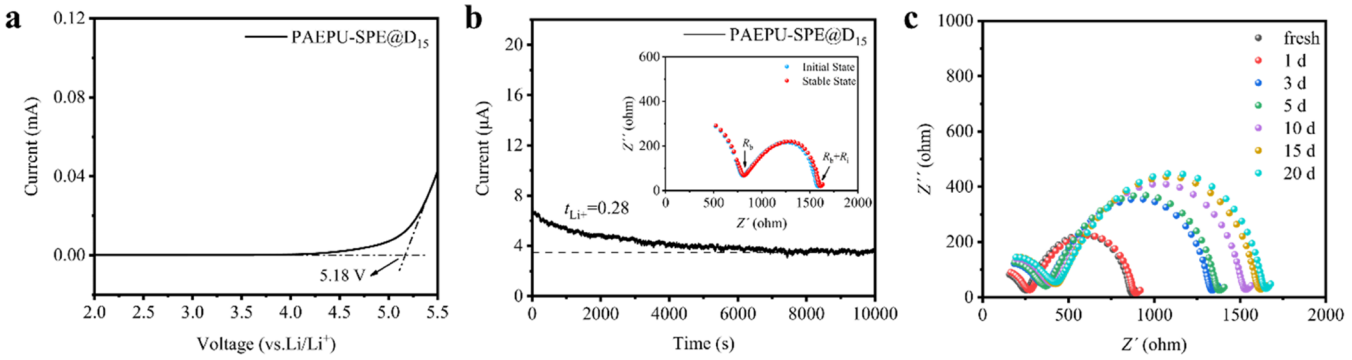

Figure 7. (a) Electrochemical stability window at room temperature. (b) Chronoamperometry profile of the Li/PAEPU-SPE@D_{15}/Li symmetric battery. The inset shows the dependence spectra before and after chronoamperometry. (c) Nyquist plots of the interfacial resistance with time for Li/PAEPU-based SPE@D_{15}/Li.

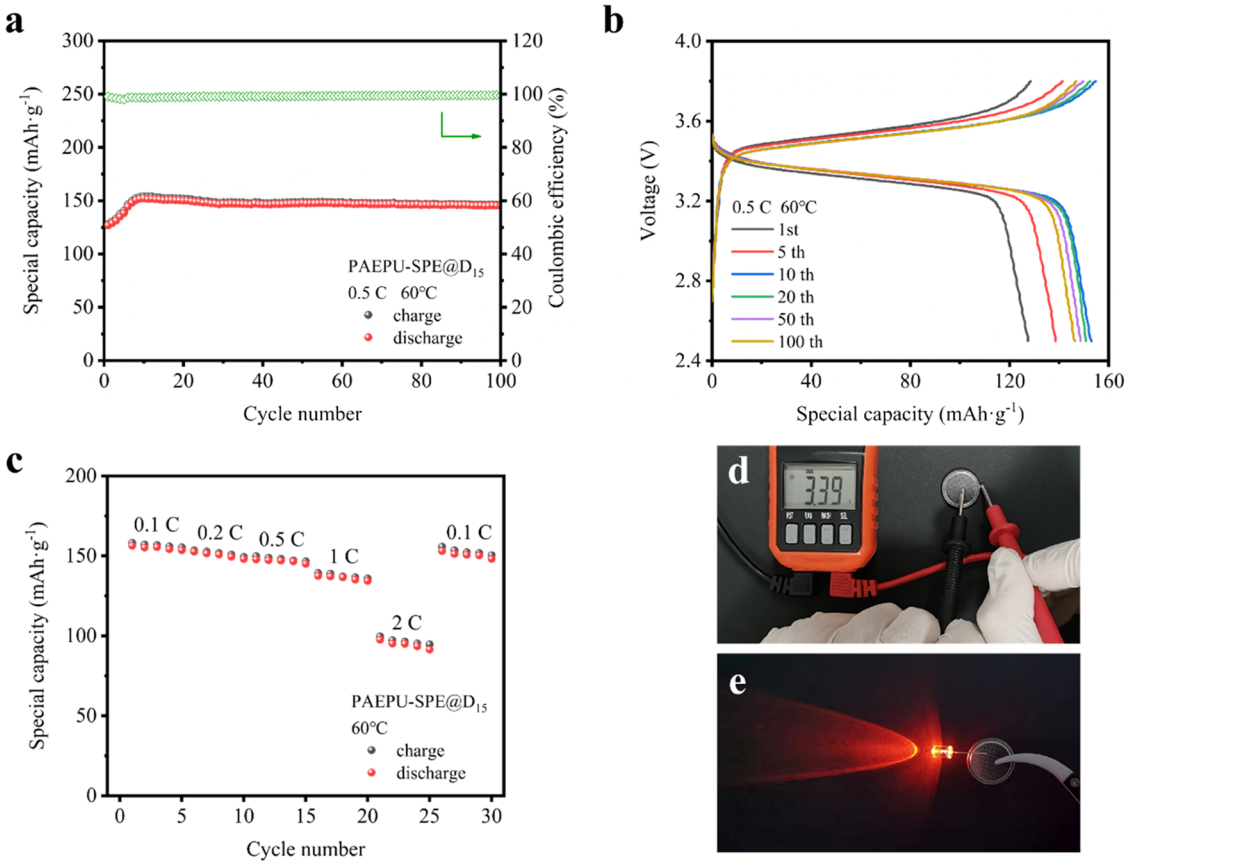

Figure 8. Electrochemical performance of the Li/PAEPU-based SPE@D_{15}/$LiFePO_4$ half-cell: (a) long cycle performance at 0.5C, 60 °C. (b) Charge and discharge curves at 0.5C, 60 °C. (c) Rate performance at different current densities at 0.5C, 60 °C. (d) DC voltage measured by a multimeter at room temperature. (e) Lighting up of a red LED lamp (1.9 V) by the assembled half-cell at room temperature.

When the LiTFSI content is 5 or 15 wt %, the ionic conductivity of the PAEPU-based SPE increased with the decrease of tri-IPDI content. When the LiTFSI is 25 wt % and the molar ratio of IPDI to tri-IPDI is 2:1, the ionic conductivity of the PAEPU-based SPE reaches the highest value, reaching 1.74×10^{-4} S cm^{-1} at 30 °C and 10^{-3} S cm^{-1} above 70 °C.

As shown in Figure 6a−c, at the same LiTFSI content, the ionic conductivity of the PAEPU-based SPE with an IPDI:tri-IPDI mole ratio of 2:1 and 3:1 is higher than that of the PAEPU-based SPE with the other three mole ratios of IPDI to tri-IPDI. Although the ionic conductivity is the highest when the LiTFSI is 25 wt %, the SPE is too soft and the morphology is not as good as that of the PAEPU-based SPE with the lithium content of 15 wt %. Considering all of the above results, the properties of PAEPU-SPE@D_{15} were determined by the following electrochemical tests.

The ionic conductivity of PAEPU-SPE@D_{15} is 6.80×10^{-5}, 2.77×10^{-4}, and 5.76×10^{-4} S cm^{-1} at 30, 60, and 80 °C, respectively. The Arrhenius equation can be used to describe the long-term transport mechanism of lithium ions in a polymer matrix. The relationship between temperature and conductivity is described by the following equation

https://doi.org/10.1021/acsomega.2c07349
ACS Omega 2023, 8, 20272−20282

$$\sigma(T) = A \exp\left(-\frac{E_a}{KT}\right)$$

where A represents the pre-factor, E_a represents the activation energy, K represents the Boltzmann constant, and T represents the thermodynamic temperature. According to the test results, the linear fitting of PAEPU-SPE@D_{15} is displayed in Figure 6d and the activation energy (E_a) of PAEPU-SPE@D_{15} is 0.40 eV.

Electrochemical stability window is an important performance index to measure the electrolyte stability. An Li//SS asymmetric cell was assembled to evaluate the electrochemical window, which was subsequently determined by linear sweep voltammetry (LSV) at room temperature; the PAEPU-SPE@D_{15} remains stable until 5.18 V (Figure 7a), demonstrating good electrochemical stability, which makes it possible to develop lithium batteries with high energy density.

The lithium-ion transference number (t_{Li^+}) was tested by EIS test and DC polarization voltage was applied to the lithium symmetric cell; the results are shown in Figure 7b. The lithium-ion transference number of PAEPU-SPE@D_{15} is 0.28, which is slightly higher than that of PEO-based polymer electrolytes (t_{Li^+} = 0.20).[64]

In this paper, the interface performance of the electrolyte/lithium metal electrode was also studied in detail. By monitoring the interface impedance of PAEPU-SPE@D_{15} at ambient temperature, the change of impedance with time was evaluated. As demonstrated in Figure 7c, the real part of the high-frequency zone is the bulk impedance (R_b) of the electrolyte, and the diameter of the arc is the interface impedance (R_i) between the electrolyte and the electrode. As time goes by, the passivation layer gradually forms and R_i also slowly increases. Significantly, the interface impedance value on the 15th day and the 20th day are almost the same, indicating that a quite stable solid electrolyte interface (SEI) has been formed. The formation of the SEI layer is conducive to the uniform deposition of lithium dendrites, and also makes the electrolyte and the electrode have good contact.

The half-cell was assembled with Li//LFP to further evaluate the electrochemical performance and feasibility of PAEPU-SPE@D_{15}. As shown in Figure 8a,b, the cycle performance was measured under the current density of 0.5C at 60 °C. Figure 8a shows that the Li/PAEPU-SPE@D_{15}/$LiFePO_4$ half-cell delivers an initial discharge capacity of 126.8 mAh g^{-1}. After seven cycles of activation, a high specific capacity 150.5 mAh g^{-1} is still obtained, and then around this value is maintained with a tremendous cycle stability. The unstable charge−discharge specific capacity in the first few cycles may be caused by the construction of the lithium-ion transport channel.[65] After 100 cycles, the discharge capacity is 145.7 mAh g^{-1}; compared with the discharge capacity of the 8th cycle, the capacity retention could reach 96.8%, and the coulombic efficiency always remained above 98.0%. Figure 8b shows the galvanostatic charge−discharge voltage profiles under the current density of 0.5C at 60 °C. Remarkably, after five charge−discharge cycles, the voltage tends to be stable, about 3.4 V, indicating that the Li/PAEPU-SPE@D_{15}/LFP had good stability. This is because the polyurea solid polymer electrolyte has a three-dimensional network structure, which is conducive to the stable performance of the battery.

Figure 8c shows the rate performance at different current densities. The discharge capacities were 156.4, 152.7, 147.8, 137.5, and 97.6 mAh g^{-1} at 0.1C, 0.2C, 0.5C, 1C, and 2C, respectively. When the current density returned to 0.1C, the reversible capacity remained at 153.1 mAh g^{-1}, with a capacity recovery rate of 97.9%, suggesting outstanding rate performance. However, the cyclic test results of the pure PEO solid polymer electrolyte at 60 °C and current densities of 0.2C,[66] 0.5C,[67,68] and 1C[68] were all lower than the specific capacity of the PAEPU-SPE prepared in this experiment. Moreover, as shown as Figure 8d,e, the DC voltage (3.39 V) was measured by a multimeter, and it could light up a red LED lamp (1.9 V) at room temperature successfully.

4. CONCLUSIONS

In summary, a series of PAEPU-based SPEs with abundant PEO chains has been designed and successfully fabricated in an in situ manner, which could achieve the integration of SPE with the polar plate, while eliminating the use of solvents. We systematically investigated the mechanics, thermal transition, and transport behaviors of PAEPU-based SPEs by varying the molar ratios of IPDI to tri-IPDI and LiTFSI concentrations and identified trends in the viscoelasticity, thermal transition, and ionic conductivity with polymer composition. The SPE displays tunable mechanical properties and ionic conductivity, excellent thermal stability ($T_{d,5}$ > 300 °C), and a low glass transition temperature (T_g < −40 °C). Additionally, at the IPDI/tri-IPDI molar ratio of 2:1 and 15 wt % LiTFSI, an optimum combination was observed in the PAEPU-based SPE system, which was used to investigate the electrochemical properties. Compared to PEO/LiTFSI, the PAEPU-based SPE displayed a higher ionic conductivity of 6.80 × 10^{-5} S cm^{-1} at 30 °C and could reach 10^{-4} orders of magnitude when the temperature was above 40 °C, with a better electrochemical stability window of 5.18 V and interface stability with lithium metal. In addition, the capacity retention rate of the Li/PAEPU-SPE@D_{15}/$LiFePO_4$ half-cell was 96.8% after 100 cycles, and in the rate test, the capacity recovery rate could reach 97.9%. The characteristics of a good interface compatibility between the electrodes and electrolyte as well as a reversible battery cycle make the solvent-free and in situ PAEPU-based SPEs one of the most promising electrolytes for next-generation all-solid-state batteries with flexible, wearable, and highly improved safety as well as economic and environmental benefits.

■ ASSOCIATED CONTENT

Supporting Information

The Supporting Information is available free of charge at https://pubs.acs.org/doi/10.1021/acsomega.2c07349.

Preparation of $LiFePO_4$ cathode and the image of PAEPU-based SPE thermal performance (PDF)

■ AUTHOR INFORMATION

Corresponding Authors

Peng Wang − *Hebei Key Laboratory of Flexible Functional Materials, School of Materials Science and Engineering, Hebei University of Science and Technology, Shijiazhuang 050000, China*; orcid.org/0000-0001-9669-9343; Email: wp390061130@126.com

Na Li − *Hebei Key Laboratory of Flexible Functional Materials, School of Materials Science and Engineering, Hebei University of Science and Technology, Shijiazhuang 050000, China*; Email: linahuaxue@163.com

Jijun Xiao − *Hebei Key Laboratory of Flexible Functional Materials, School of Materials Science and Engineering, Hebei*

https://doi.org/10.1021/acsomega.2c07349
ACS Omega 2023, 8, 20272−20282

University of Science and Technology, Shijiazhuang 050000, China; Email: xiaojj@hebust.edu.cn

Authors

Lu Bai − *Hebei Key Laboratory of Flexible Functional Materials, School of Materials Science and Engineering, Hebei University of Science and Technology, Shijiazhuang 050000, China; Institute of Energy Source, Hebei Academy of Sciences, Shijiazhuang 050052, China*

Chengyu Li − *Hebei Key Laboratory of Flexible Functional Materials, School of Materials Science and Engineering, Hebei University of Science and Technology, Shijiazhuang 050000, China*

Xiaoqi Chen − *Institute of Energy Source, Hebei Academy of Sciences, Shijiazhuang 050052, China*

Yantao Li − *Institute of Energy Source, Hebei Academy of Sciences, Shijiazhuang 050052, China*

Complete contact information is available at: https://pubs.acs.org/10.1021/acsomega.2c07349

Author Contributions

[§]L.B. and P.W. contributed equally to this work.

Notes

The authors declare no competing financial interest.

■ ACKNOWLEDGMENTS

The authors gratefully acknowledge the financial support from the National Natural Science Foundation of China (nos. 52174287, 5210011286, and 51904343), Science and Technology Program of Hunan Province (no. 2019RS3002), Funds for Creative Research Groups of Hunan province (no. 2020JJ1007), the Hebei Provincial Natural Science Foundation (E2021208031, B2021208069), and the Fundamental Research Funds for the Hebei University (2021YWF11).

■ REFERENCES

(1) Fan, E.; Li, L.; Wang, Z.; Lin, J.; Huang, Y.; Yao, Y.; Chen, R.; Wu, F. Sustainable Recycling Technology for Li-ion Batteries and Beyond: Challenges and Future Prospects. *Chem. Rev.* **2020**, *120*, 7020−7063.

(2) Xia, S.; Wu, X.; Zhang, Z.; Cui, Y.; Liu, W. Practical Challenges and Future Perspectives of All-Solid-State Lithium-Metal Batteries. *Chem* **2019**, *5*, 753−785.

(3) Wang, Q.; Cui, Z.; Zhou, Q.; Shangguan, X.; Du, X.; Dong, S.; Qiao, L.; Huang, S.; Liu, X.; Tang, K.; et al. A Supramolecular Interaction Strategy Enabling High-Performance All Solid State Electrolyte of Lithium Metal Batteries. *Energy Storage Mater.* **2020**, *25*, 756−763.

(4) Wu, F.; Maier, J.; Yu, Y. Guidelines and Trends for Next-Generation Rechargeable Lithium and Lithium-Ion Batteries. *Chem. Soc. Rev.* **2020**, *49*, 1569−1614.

(5) Yue, L.; Ma, J.; Zhang, J.; Zhao, J.; Dong, S.; Liu, Z.; Cui, G.; Chen, L. All Solid-State Polymer Electrolytes for High-Performance Lithium Ion Batteries. *Energy Storage Mater.* **2016**, *5*, 139−164.

(6) Piedrahita, C.; Kusuma, V.; Nulwala, H. B.; Kyu, T. Highly Conductive, Flexible Polymer Electrolyte Membrane Based on Poly(ethylene glycol) Diacrylate-co-Thiosiloxane Network. *Solid State Ionics* **2018**, *322*, 61−68.

(7) Wang, Q.; Mao, B.; Stoliarov, S. I.; Sun, J. A Review of Lithium Ion Battery Failure Mechanisms and Fire Prevention Strategies. *Prog. Energy Combust. Sci.* **2019**, *73*, 95−131.

(8) Feng, X.; Ouyang, M.; Liu, X.; Lu, L.; Xia, Y.; He, X. Thermal Runaway Mechanism of Lithium Ion Battery for Electric Vehicles: A Review. *Energy Storage Mater.* **2018**, *10*, 246−267.

(9) Zhou, J.; Qian, T.; Liu, J.; Wang, M.; Zhang, L.; Yan, C. High Safety All-Solid-State Lithium Metal Battery with High Ionic Conductivity Thermoresponsive Solid Polymer Electrolyte. *Nano Lett.* **2019**, *19*, 3066−3073.

(10) Tianwei, Y.; Xiaofei, Y.; Rong, Y.; Xiangtao, B.; Guofeng, X.; Shangqian, Z.; Yi, D.; Yanlong, W.; Jiantao, W. Progress and Perspectives on Typical Inorganic Solid-State Electrolytes. *J. Alloys Compd.* **2021**, *885*, No. 161013.

(11) Karabelli, D.; Peter, B. K.; Max, W. A Performance and Cost Overview of Selected Solid-State Electrolytes: Race between Polymer Electrolytes and Inorganic Sulfide Electrolytes. *Batteries* **2021**, *7*, No. 18.

(12) Guan, X.; Min, X.; Shuanjin, W.; Dongmei, H.; Yuning, L.; Yuezhong, M. Polymer-Based Solid Electrolytes: Material Selection, Design, and Application. *Adv. Funct. Mater.* **2020**, *31*, No. 2007598.

(13) Fengquan, L.; Fengjuan, B.; Jinxin, X.; Lu, W.; Yujie, Y.; Hong, H.; Jianjun, Z.; Lin, L. Polymer Electrolyte Membrane with High Ionic Conductivity and Enhanced Interfacial Stability for Lithium Metal Battery. *ACS Appl. Mater. Interfaces* **2020**, *12*, 22710−22720.

(14) Zeng, F.; Sun, Y.; Hui, B.; Xia, Y.; Zou, Y.; Zhang, X.; Yang, D. Three-Dimensional Porous Alginate Fiber Membrane Reinforced PEO-Based Solid Polymer Electrolyte for Safe and High-Performance Lithium Ion Batteries. *ACS Appl. Mater. Interfaces* **2020**, *12*, 43805−43812.

(15) Zeng, D.; Yao, J.; Zhang, L.; Xu, R.; Wang, S.; Yan, X.; Yu, C.; Wang, L. Promoting Favorable Interfacial Properties in Lithium-Based Batteries Using Chlorine-Rich Sulfide Inorganic Solid-State Electrolytes. *Nat. Commun.* **2022**, *13*, No. 1909.

(16) Wang, H.; Sheng, L.; Yasin, G.; Wang, L.; Xu, H.; He, X. Reviewing the Current Status and Development of Polymer Electrolytes for Solid-State Lithium Batteries. *Energy Storage Mater.* **2020**, *33*, 188−215.

(17) Wang, Q.; Zhang, H.; Cui, Z.; Zhou, Q.; Shangguan, X.; Tian, S.; Zhou, X.; Cui, G. Siloxane-Based Polymer Electrolytes for Solid-State Lithium Batteries. *Energy Storage Mater.* **2019**, *23*, 466−490.

(18) Fang, F.; Wei, L.; Yue, Z.; Kai, C.; Chen, S.; Lina, C.; Yulong, L.; Haiming, X.; Liqun, S. Regulating Lithium Deposition via Bifunctional Regular-Random Cross-Linking Network Solid Polymer Electrolyte for Li Metal Batteries. *J. Power Sources* **2021**, *484*, No. 229186.

(19) Lopez, J.; Mackanic, D. G.; Cui, Y.; Bao, Z. Designing Polymers for Advanced Battery Chemistries. *Nat. Rev. Mater.* **2019**, *4*, 312−330.

(20) Xue, Z.; He, D.; Xie, X. Poly(ethylene oxide)-Based Electrolytes for Lithium-Ion Batteries. *J. Mater. Chem. A* **2015**, *3*, 19218−19253.

(21) Jeedi, V. R.; Narsaiah, E. L.; Yalla, M.; Swarnalatha, R.; Reddy, S. N.; Sadananda Chary, A. Structural and Electrical Studies of PMMA and PVDF Based Blend Polymer Electrolyte. *SN Appl. Sci.* **2020**, *2*, 1−10.

(22) Tran, H. K.; Wu, Y.-S.; Chien, W.-C.; Wu, S.-h.; Jose, R.; Lue, S. J.; Yang, C.-C. Composite Polymer Electrolytes Based on PVA/PAN for All-Solid-State Lithium Metal Batteries Operated at Room Temperature. *ACS Appl. Energy Mater.* **2020**, *3*, 11024−11035.

(23) Kang, S.; Yang, C.; Yang, Z.; Wu, N.; Shi, B.; et al. Blending Based PEO-PAN-PMMA Gel Polymer Electrolyte Prepared by Spaying Casting for Solid-State Lithium Metal Batteries. *Acta Chin. Sin.* **2020**, *78*, No. 1441.

(24) Yao, Z.; Zhu, K.; Li, X.; Zhang, J.; Chen, J.; Wang, J.; Yan, K.; Liu, J. 3D Poly(vinylidene fluoride-hexafluoropropylen) Nanofiber-Reinforced PEO-Based Composite Polymer Electrolyte for High-Voltage Lithium Metal Batteries. *Electrochim. Acta* **2021**, *404*, No. 139769.

(25) Olmedo-Martínez, J. L.; Porcarelli, L.; Guzmán-González, G.; Calafel, I.; Forsyth, M.; Mecerreyes, D.; Müller, A. J. Ternary Poly(ethylene oxide)/Poly($_{L,L}$-lactide) PEO/PLA Blends as High-Temperature Solid Polymer Electrolytes for Lithium Batteries. *ACS Appl. Polym. Mater.* **2021**, *3*, 6326−6337.

(26) Aadheeshwaran, S.; Sankaranarayanan, K. Electrochemical Behavior of $BaTiO_3$ Embedded Spongy PVDF-HFP/Cellulose

Blend as a Novel Gel Polymer Electrolyte for Lithium-Ion Batteries. *Mater. Lett.* **2022**, *306*, No. 130938.
(27) Bergfelt, A.; Rubatat, L.; Brandell, D.; Bowden, T. Poly(benzyl methacrylate)-Poly[(oligo ethylene glycol) Methyl Ether Methacrylate] Triblock-Copolymers as Solid Electrolyte for Lithium Batteries. *Solid State Ionics* **2018**, *321*, 55−61.
(28) Young, N. P.; Devaux, D.; Khurana, R.; Coates, G. W.; Balsara, N. P. Investigating Polypropylene-Poly(ethylene oxide)-Polypropylene Triblock Copolymers as Solid Polymer Electrolytes for Lithium Batteries. *Solid State Ionics* **2014**, *263*, 87−94.
(29) Zardalidis, G.; Gatsouli, K.; Pispas, S.; Mezger, M.; Floudas, G. Ionic Conductivity, Self-Assembly, and Viscoelasticity in Poly(styrene-b-ethylene oxide) Electrolytes Doped with LiTf. *Macromolecules* **2015**, *48*, 7164−7171.
(30) Butzelaar, A. J.; Roring, P.; Mach, T. P.; Hoffmann, M.; Jeschull, F.; Wilhelm, M.; Winter, M.; Brunklaus, G.; Théato, P. Styrene-Based Poly(ethylene oxide) Side-Chain Block Copolymers as Solid Polymer Electrolytes for High-Voltage Lithium-Metal Batteries. *ACS Appl. Mater. Interfaces* **2021**, *13*, 39257−39270.
(31) Zhu, Y.; Cao, S.; Huo, F. Molecular Dynamics Simulation Study of the Solid Polymer Electrolyte that PEO Grafted POSS. *Chem. Phys. Lett.* **2020**, *756*, No. 137834.
(32) Li, S.; Jiang, K.; Wang, J.; Zuo, C.; Xue, Z.; et al. Molecular Brush with Dense PEG Side Chains: Design of a Well-Defined Polymer Electrolyte for Lithium-Ion Batteries. *Macromolecules* **2019**, *52*, 7234−7243.
(33) Xu, S.; Sun, Z.; Sun, C.; Li, F.; Chen, K.; Zhang, Z.; Hou, G.; Cheng, H. M.; Li, F. Homogeneous and Fast Ion Conduction of PEO-Based Solid-State Electrolyte at Low Temperature. *Adv. Funct. Mater.* **2020**, *30*, No. 2007172.
(34) Huang, Z.; Pan, Q.; Smith, D. M.; Li, C. Y. Plasticized Hybrid Network Solid Polymer Electrolytes for Lithium-Metal Batteries. *Adv. Mater. Interfaces* **2019**, *6*, No. 1801445.
(35) Jinisha, B.; Anilkumar, K.; Manoj, M.; Pradeep, V.; Jayalekshmi, S. Development of a Novel Type of solid Polymer Electrolyte for Solid State Lithium Battery Applications Based on Lithium Enriched Poly(ethylene oxide) (PEO)/Poly(vinyl pyrrolidone) (PVP) Blend Polymer. *Electrochim. Acta* **2017**, *235*, 210−222.
(36) Tao, C.; Gao, M. H.; Yin, B. H.; Li, B.; Huang, Y. P.; Xu, G.; Bao, J. J. A Promising TPU/PEO Blend Polymer Electrolyte for All-Solid-State Lithium Ion Batteries. *Electrochim. Acta* **2017**, *257*, 31−39.
(37) Pan, X.; Yang, P.; Guo, Y.; Zhao, K.; Xi, B.; Lin, F.; Xiong, S. Electrochemical and Nanomechanical Properties of TiO_2 Ceramic Filler Li-Ion Composite Gel Polymer Electrolytes for Li Metal Batteries. *Adv. Mater. Interfaces* **2021**, *8*, No. 2100669.
(38) Mengistie, T. S.; Ko, J. M.; Kim, J. Y. Enhanced Single-Ion Conduction and Free-Standing Properties of Solid Polymer Electrolyte by Incorporating a Polyelectrolyte. *Mater. Res. Express* **2021**, *8*, No. 035308.
(39) Ling, C. K.; Aung, M. M.; Rayung, M.; Abdullah, L. C.; Lim, H. N.; Mohd Noor, I. S. Performance of Ionic Transport Properties in Vegetable Oil-Based Polyurethane Acrylate Gel Polymer Electrolyte. *ACS Omega* **2019**, *4*, 2554−2564.
(40) Kalybekkyzy, S.; Kopzhassar, A.-F.; Kahraman, M. V.; Mentbayeva, A.; Bakenov, Z. Fabrication of UV-Crosslinked Flexible Solid Polymer Electrolyte with PDMS for Li-Ion Batteries. *Polymers* **2021**, *13*, No. 15.
(41) Cai, M.; Zhu, J.; Yang, C.; Gao, R.; Shi, C.; Zhao, J. A Parallel Bicomponent TPU/PI Membrane with mechanical Strength Enhanced Isotropic Interfaces used as Polymer Electrolyte for Lithium-Ion Battery. *Polymers* **2019**, *11*, No. 185.
(42) Xu, P.; Chen, H.; Zhou, X.; Xiang, H. Gel Polymer Electrolyte Based on PVDF-HFP Matrix Composited with rGO-PEG-NH_2 for High-Performance Lithium Ion Battery. *J. Membr. Sci.* **2021**, *617*, No. 118660.
(43) Zaheer, M.; Xu, H.; Wang, B.; Li, L.; Deng, Y. An In Situ Polymerized Comb-Like PLA/PEG-Based Solid Polymer Electrolyte for Lithium Metal Batteries. *J. Electrochem. Soc.* **2019**, *167*, No. 070504.
(44) Mohamed, N.; Arof, A. Investigation of Electrical and Electrochemical Properties of PVDF-Based Polymer Electrolytes. *J. Power Sources* **2004**, *132*, 229−234.
(45) Sun, J.; Li, Y.; Zhang, Q.; Hou, C.; Shi, Q.; Wang, H. A Highly Ionic Conductive Poly(methyl methacrylate) Composite Electrolyte with Garnet-Typed $Li_{6.75}La_3Zr_{1.75}Nb_{0.25}O_{12}$ Nanowires. *Chem. Eng. J.* **2019**, *375*, No. 121922.
(46) Wang, Z.; Shen, L.; Deng, S.; Cui, P.; Yao, X. 10 μm-Thick High-Strength Solid Polymer Electrolytes with Excellent Interface Compatibility for Flexible All-Solid-State Lithium-Metal Batteries. *Adv. Mater.* **2021**, *33*, No. 2100353.
(47) Liu, B.; Huang, Y.; Zhao, L.; Huang, Y.; Song, A.; Lin, Y.; Wang, M.; Li, X.; Cao, H. A Novel Non-Woven Fabric Supported Gel Polymer Electrolyte Based on Poly(methylmethacrylate-polyhedral oligomeric silsesquioxane) by Phase Inversion Method for Lithium Ion Batteries. *J. Membr. Sci.* **2018**, *564*, 62−72.
(48) Zhao, Y.; Zhang, Y.; Bakenov, Z.; Chen, P. Electrochemical Performance of Lithium Gel Polymer Battery with Nanostructured Sulfur/Carbon Composite Cathode. *Solid State Ionics* **2013**, *234*, 40−45.
(49) Gan, H.; Li, S.; Zhang, Y.; Wang, J.; Xue, Z. Electrospun Composite Polymer Electrolyte Membrane Enabled with Silica-Coated Silver Nanowires. *Eur. J. Inorg. Chem.* **2021**, *2021*, 4639−4646.
(50) Janakiraman, S.; Surendran, A.; Ghosh, S.; Anandhan, S.; Venimadhav, A. A New Strategy of PVDF Based Li-Salt Polymer Electrolyte Through Electrospinning for Lithium Battery Application. *Mater. Res. Express* **2019**, *6*, No. 035303.
(51) Chai, J.; Liu, Z.; Ma, J.; Wang, J.; Liu, X.; Liu, H.; Zhang, J.; Cui, G.; Chen, L. In Situ Generation of Poly(vinylene carbonate) Based Solid Electrolyte with Interfacial Stability for $LiCoO_2$ Lithium Batteries. *Adv. Sci.* **2017**, *4*, No. 1600377.
(52) Wei, J.; Yue, H.; Shi, Z.; Li, Z.; Li, X.; Yin, Y.; Yang, S. In Situ Gel Polymer Electrolyte with Inhibited Lithium Dendrite Growth and Enhanced Interfacial Stability for Lithium-Metal Batteries. *ACS Appl. Mater. Interfaces* **2021**, *13*, 32486−32494.
(53) Sun, M.; Zeng, Z.; Peng, L.; Han, Z.; Yu, C.; Cheng, S.; Xie, J. Ultrathin Polymer Electrolyte Film Prepared by In Situ Polymerization for Lithium Metal Batteries. *Mater. Today Energy* **2021**, *21*, No. 100785.
(54) Choudhury, S.; Stalin, S.; Vu, D.; Warren, A.; Deng, Y.; Biswal, P.; Archer, L. A. Solid-State Polymer Electrolytes for High-Performance Lithium Metal Batteries. *Nat. Commun.* **2019**, *10*, No. 4398.
(55) Fu, F.; Lu, W.; Zheng, Y.; Chen, K.; Sun, C.; Cong, L.; Liu, Y.; Xie, H.; Sun, L. Regulating Lithium Deposition via Bifunctional Regular-Random Cross-Linking Network Solid Polymer Electrolyte for Li Metal Batteries. *J. Power Sources* **2021**, *484*, No. 229186.
(56) Liu, Z.; Guo, D.; Fan, W.; Xu, F.; Yao, X. Expansion-Tolerant Lithium Anode with Built-In LiF-Rich Interface for Stable 400 Wh kg^{-1} Lithium Metal Pouch Cells. *ACS Mater. Lett.* **2022**, *4*, 1516−1522.
(57) Liu, M.; Zhang, S.; Li, G.; Wang, C.; Li, B.; Li, M.; Wang, Y.; Ming, H.; Wen, Y.; Qiu, J.; et al. A Cross-Linked Gel Polymer Electrolyte Employing Cellulose Acetate Matrix and Layered Boron Nitride Filler Prepared via In Situ Thermal Polymerization. *J. Power Sources* **2021**, *484*, No. 229235.
(58) Drews, M.; Trötschler, T.; Bauer, M.; Guntupalli, A.; Beichel, W.; Gentischer, H.; Mülhaupt, R.; Kerscher, B.; Biro, D. Photocured Cationic Polyoxazoline Macromonomers as Gel Polymer Electrolytes for Lithium-Ion Batteries. *ACS Appl. Polym. Mater.* **2022**, *4*, 158−168.
(59) Yu, F.; Zhang, H.; Zhao, L.; Sun, Z.; Li, Y.; Mo, Y.; Chen, Y. A Flexible Cellulose/Methylcellulose Gel Polymer Electrolyte Endowing Superior Li^+ Conducting Property for Lithium Ion Battery. *Carbohydr. Polym.* **2020**, *246*, No. 116622.
(60) Hess, H.; Kopp, R.; Groglerl, G.; Stepanski, H.; Hombach, R.; Schafer, W. Polyurethane-Based Reactive Adhesives in Which the Isocyanate is Stabilized by a Polyether Amine. U.S. Patent, US5,104,959A1992.

https://doi.org/10.1021/acsomega.2c07349
ACS Omega 2023, 8, 20272−20282

(61) Pimenta, A. S.; Trianoski, R.; Pizzi, A.; Santiago-Medina, F. J.; de Souza, E. C.; Monteiro, T. V. d. C.; Fasciotti, M.; Castro, R. V. O. Effect of Polymeric Diisocyanate Addition on Bonding Performance of a Demethylated-Pyrolysis-Oil-Based Adhesive. *Wood Sci. Technol.* **2019**, *53*, 1311−1337.
(62) Xu, H.; Zhang, X.; Hu, G.; Weng, L.; Liu, L. High Thermal Conductivity EP Adhesive Based on the GO/EP Interface Optimized by TDI. *Polym. Adv. Technol.* **2020**, *31*, 1356−1364.
(63) Jang, H. K.; Jung, B. M.; Choi, U. H.; Lee, S. B. Ion Conduction and Viscoelastic Response of Epoxy-Based Solid Polymer Electrolytes Containing Solvating Plastic Crystal Plasticizer. *Macromol. Chem. Phys.* **2018**, *219*, No. 1700514.
(64) Chen, B.; Huang, Z.; Chen, X.; Zhao, Y.; Xu, Q.; Long, P.; Chen, S.; Xu, X. A New Composite Solid Electrolyte PEO/$Li_{10}GeP_2S_{12}$/SN for All-Solid-State Lithium Battery. *Electrochim. Acta* **2016**, *210*, 905−914.
(65) Zhang, D.; Xu, X.; Ji, S.; Wang, Z.; Liu, Z.; Shen, J.; Hu, R.; Liu, J.; Zhu, M. Solvent-Free Method Prepared a Sandwich-Like Nanofibrous Membrane-Reinforced Polymer Electrolyte for High-Performance All-Solid-State Lithium Batteries. *ACS Appl. Mater. Interfaces* **2020**, *12*, 21586−21595.
(66) Tan, J.; Ao, X.; Dai, A.; Yuan, Y.; Zhuo, H.; Lu, H.; Zhuang, L.; Ke, Y.; Su, C.; Peng, X.; et al. Polycation Ionic Liquid Tailored Peo-Based Solid Polymer Electrolytes for High Temperature Lithium Metal Batteries. *Energy Storage Mater.* **2020**, *33*, 173−180.
(67) Zhu, L.; Zhu, P.; Fang, Q.; Jing, M.; Shen, X.; Yang, L. A Novel Solid PEO/LLTO-Nanowires Polymer Composite Electrolyte for Solid-State Lithium-Ion Battery. *Electrochim. Acta* **2018**, *292*, 718−726.
(68) Wen, J.; Zhao, Q.; Jiang, X.; Ji, G.; Wang, R.; Lu, G.; Long, J.; Hu, N.; Xu, C. Graphene Oxide Enabled Flexible PEO-Based Solid Polymer Electrolyte for All-Solid-State Lithium Metal Battery. *ACS Appl. Energy Mater.* **2021**, *4*, 3660−3669.

https://doi.org/10.1021/acsomega.2c07349
ACS Omega 2023, 8, 20272−20282